

Studying Wave optics in exoplanet microlensing light curves

Ahmad Mehrabi¹ and Sohrab Rahvar^{1,2} *

¹ *Department of Physics, Sharif University of Technology, P.O.Box 11365–9161, Tehran, Iran*

² *Perimeter Institute for Theoretical Physics, 31 Caroline Street North, Waterloo, Ontario N2L 2Y5, Canada*

18 July 2012

ABSTRACT

We study the wave optics feature of the gravitational microlensing by a binary system composed of parent star and a planet. In the binary system, near the caustic lines multiple images play the role of secondary sources for the observer, in analogy to the double slit Young's experiment. In the case of having coherent wave fronts from the source on the lens plane, images can produce diffraction pattern on the observer plane. For the binary lensing system we have two modes of close and wide images around the planet and lens star and these images can produce two different types of fringes with the high and low frequencies on the observer plane. By taking into account the finite size of the source star, enhancements in the diffraction fringes get dimmer. For the observational prospects, we study this effect for the SKA project in the case of resonance and the high magnification exoplanet channels. This method can partially break degeneracies between the lens parameters.

1 INTRODUCTION

Gravitational lensing addresses to the bending of light rays by the gravitational effect of foreground mass. Depending on the distribution of mass on the lens plane and the relative location of the lens and source from the observer, multiple images or distortion of the background source can be formed. In the case of star-star lensing inside the Milky Way, the separation of the images are less than few milliarsecond hence they are unresolvable for the ground based telescopes. This type of gravitational lensing is so-called gravitational microlensing.

In 1936 Einstein derived the gravitational lensing equation, but it took several years until 1979 that first gravitational lensing was observed. The source of this lensing was a quasar and observation was done in the radio frequencies (Walsh et al 1979). A few years later Paczyński proposed studying MACHO's ¹ population in the Galactic halo by the gravitational microlensing (Paczynski 1986). His suggestion was observing stars in the Large and Small Magellanic Clouds and by counting the number of microlensing events and measuring the transit time (Einstein crossing time), it would be possible to obtain the contribution of MACHOs in the Galactic halo. Beside the dark matter studies, the other interesting astrophysical application of microlensing was suggested by Moa and Paczynski (1991), using gravitational microlensing for the discovery of exoplanets.

The microlensing effect by single or multiple lenses was mainly studied in the geometric optics. An important study on the wave optics feature of the gravitational lensing was done by Ohanian (1983) who investigated the amplification of a radio point source when a galaxy acts as a gravitational lens. He showed that wave optics smoothes singular features of the light curve in the caustic crossing. In another work, Jaroszyński and Paczyński (1995) studied the caustic crossing of object like Q2237+0305 by a galaxy

composed by the individual stars. Studying the diffraction images of this system could put limit on the size of source. In Galactic scales the observation of the wave optics features also has astrophysical application as studying the limb darkening of the small size sources as white dwarfs (Zabel & Peterson 2003). Recently Heyl (2010, 2011a, 2011b) argued about the possibility of detection of wave optics signals by the individual sub-stellar objects in the microlensing light curve.

In this work our aim is to extend the application of the wave optics to the conventional observation of extra solar planets by the gravitational microlensing. Here we take a binary system composed of a lensing star and planet. Crossing the caustic lines of this system by the source star, produces high magnification in the light curve. For some of the cases due to the small separation of the images on the lens plane, the gravitational lensing system resembles to a multiple slit optical system in the astronomical scales. Having coherent condition for the wave fronts on the lens plane, the result would be a diffraction pattern on the observer plane. We study the application of this method both for the resonance and high magnification channels of the exoplanet observations. The observation of the enhancements and transition of the fringes will enable us to break degeneracy of the lens parameters. We also study the prospect of observation of the wave optics signal by future Square Kilometer Array (SKA) project.

In section (2), we used the wave optics formalism and calculate the light curve of a point like and the extended source, lensed by a binary system. In section (3) we perform semi-analytic approach of the wave optics in the microlensing near the fold caustics and study the conditions having the wave optics features. In section (4) we discuss about the possibility of detection of wave optics signature of the extra-solar planets in the radio and micrometer emissions of the source stars and prospect the observation of the light curves by SKA. We also discuss on the physical parameters that we can get from the light curve and degeneracy breaking

¹ Massive Astrophysical Compact Halo Objects

in the resonance and high magnification channels. The conclusion and summary is given in section (5).

2 WAVE OPTICS IN GRAVITATIONAL LENSING

In the geometrical optics, the locations of the images can be obtained from solving the lens equation

$$\mathbf{y} = \mathbf{x} - \alpha(\mathbf{x}), \quad (1)$$

where \mathbf{x} is the angular location of the the image, \mathbf{y} is the angular position of the source and $\alpha(x)$ is the deflection, given by

$$\alpha(\mathbf{x}) = \frac{1}{\pi} \int \kappa(\mathbf{x}') \frac{\mathbf{x} - \mathbf{x}'}{|\mathbf{x} - \mathbf{x}'|^2} d^2 x', \quad (2)$$

where $\kappa(x) = \Sigma(x)/\Sigma_{cr}$, $\Sigma_{cr}^{-1} = (4\pi G D_d D_{ds})/(c^2 D_s)$ and D_s , D_{ds} , D_d are the source, lens-source and lens distances, respectively. $\Sigma(x)$ is the surface mass density of the lens. Another way to get the position of the images from the position of the source is using the Fermat principle. For the stationary points of the Fermat potential, the position of the images obtain as

$$\nabla_{\mathbf{x}} \phi(\mathbf{x}, \mathbf{y}) = 0, \quad (3)$$

where Fermat potential is given by

$$\phi(\mathbf{x}, \mathbf{y}) = \frac{1}{2}(\mathbf{y} - \mathbf{x})^2 - \psi(\mathbf{x}), \quad (4)$$

and deflection angle is

$$\alpha(\mathbf{x}) = \nabla_{\mathbf{x}} \psi(\mathbf{x}). \quad (5)$$

Here \mathbf{x} and \mathbf{y} are the image and source positions on the lens plane, normalized to the projected Einstein radius in each plane. Using the determinant of Jacobian transformation $J(x_i)$, we can obtain the magnification of a point like source mapping from the lens plane as follows:

$$\mu(x_i) = \frac{1}{|\det J(x_i)|} = \frac{1}{|\phi_{11}(x_i)\phi_{22}(x_i) - \phi_{12}^2(x_i)|}, \quad (6)$$

where x_i is location of i th image. For an extended source, we can calculate the magnification over source area. There are advance numerical methods such as using Green's theorem where two dimensional integration over the source transfer to one dimensional integration on the boundary of images (Dominik 2007).

In the wave optics, from the Huygens principle, every point on the lens plane can be considered as a secondary source and the amplitude of the electromagnetic wave on each point of the observer plane is composed by the superposition of the infinitesimal sources on the lens plane. From the Kirchhoff integral we can obtain the amplitude of the electromagnetic wave $F_{\mu\nu}$, knowing the boundary condition on the lens plane and when the distance to the observer screen is large compare to the wave length, (Born and Wolf 2002). Multiplying the overlapped electro-magnetic field to its complex conjugate results in the magnification of the light on the observer plane as follows (Schneider et al. 1992):

$$\mu(\mathbf{y}) = \frac{f^2}{4\pi^2} \left| \int e^{if\phi(\mathbf{x}, \mathbf{y})} d^2 x \right|^2 \quad (7)$$

where $f\phi(\mathbf{x}, \mathbf{y})$ corresponds to the elapsed phase for the electromagnetic wave emitted from source, deflected from x and received by the observer. $f = 2kR_s$ and $R_s = 2GM_t/c^2$ is the Schwarzschild radius of the total masses. This formula is obtained for a monochromatic electromagnetic wave.

In order to show the compatibility of the wave optics with the geometric optics and also transition from the wave optics to the geometric optics, we do Taylor expansion of the Fermat potential on the lens plane. For a given location of the source, the expansion around the image is given by

$$\begin{aligned} \phi(\mathbf{x}, \mathbf{y}) &= \phi^{(0)} + (\mathbf{x} - \mathbf{x}_i) \cdot \nabla_{\mathbf{x}} \phi^{(0)} + \frac{1}{2}[(x_1 - x_{1i})^2 \phi_{11}^{(0)} \\ &+ (x_2 - x_{2i})^2 \phi_{22}^{(0)} + 2(x_1 - x_{1i})(x_2 - x_{2i})\phi_{21}^{(0)}] + \dots \end{aligned} \quad (8)$$

where "naught" superscript represent the Fermat potential at the position of the image and subscript represent the derivative with respect to the axes on the lens plane. Substitute it in equation (7), the first term after multiplication of $\exp[i\phi(\mathbf{x}_i, \mathbf{y}_i)]$ to the complex conjugate results in unity. The second term is zero from the Fermat principle and finally the third term as non-zero term results in magnification in the geometric optics as equation (6). For the third order ϕ_{ijk} and higher orders of derivatives, the Fermat potential results in the optical wave feature in the light curve.

One of the important issues in the wave optics is that, in reality, sources are not completely coherent and we may define a coherent time scale of $\Delta\tau = \Delta\omega^{-1}$, where $\Delta\omega$ is the width of the spectrum. In this case the amplitude of the wave on the observer plane emitted from \mathbf{y} is given by

$$V(\mathbf{x}, \mathbf{y}, \phi) \propto \int g(\omega) e^{i2R_s \phi(\mathbf{x}, \mathbf{y})\omega} d\omega,$$

and the magnification, taking into account the spectrum of the source is given by:

$$\mu(\mathbf{y}) = \frac{R_s^2}{\pi^2} \left| \int d^2 x \int g(\omega) e^{2iR_s \phi(\mathbf{x}, \mathbf{y})\omega} d\omega \right|^2, \quad (9)$$

here we set the speed of light, $c = 1$. For a coherent monochromatic source $g(\omega) = \omega\delta(\omega - \omega_0)$, substituting in equation (9), we recover equation (7). Assuming a non-zero temperature for a source, the Doppler broadening changes the spectrum of the source to a Gaussian distribution with the width of $\Delta\omega$ at a given emission line. The effect of incoherent light is diminishing wave optics effect, results the wave optics approaches to the geometric optics feature.

An important point regarding the validity of the wave optics is the coherency of the light arriving to the observer plane from different images on the lens plane (Mandzhos 1981). In addition, each image should also have coherent light receiving from an extended source. We will discuss this point in the finite size effect sub-section. Assuming that source is located infinitely far from the lens plane and has zero angular size, to examine the coherency of different images interfere on the source plane, we obtain the time delay between the two rays on the lens plane and compare it with the coherent time of the source. For a point source, time difference between the two rays received by the observer through the images are

$$\Delta t = 2R_s [\phi(\mathbf{x}_{I1}, \mathbf{y}) - \phi(\mathbf{x}_{I2}, \mathbf{y})], \quad (10)$$

where the source location is fixed and \mathbf{x}_{I1} and \mathbf{x}_{I2} are the location of the images. The difference between the two Fermat potentials, $\Delta\phi$ for two far images is in the order one. For the case of two images generated during the caustic crossing, $\Delta\phi$ could be in the order of 10^{-3} . If we quantify the time delay for the wide and close images in the caustic crossing, they are given as follows:

$$\Delta t \sim 1 \times 2R_s \sim 10^{-5} \frac{M}{M_\odot} \text{ sec}, \quad (11)$$

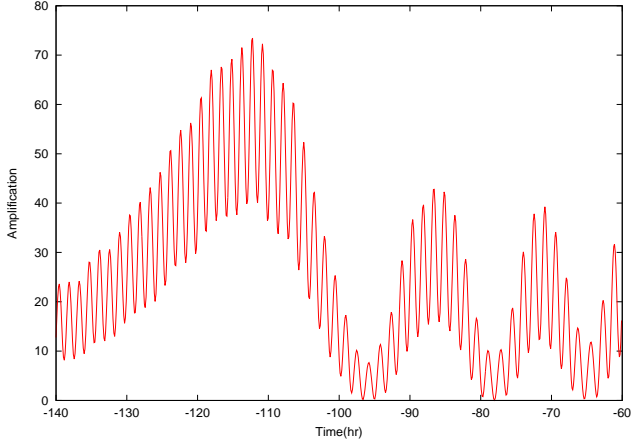


Figure 1. The light curve of a point like coherent source with the parameters $d = 0.8$, $q = 0.1$, $u_0 = 0$, $\alpha = 0$, $t_E = 20$ days, $f = 1000$

and

$$\Delta t \sim 0.001 \times 2R_s \sim 10^{-8} \frac{M}{M_\odot} \text{ sec.} \quad (12)$$

We will discuss about these formulas in detail at section (3), as the source gets closer to the caustic line (i.e. $\Delta t \rightarrow 0$). For a source with non-zero temperature of T , relation between the coherent time and the bandwidth of the spectrum is given by $\tau_c \Delta \omega \sim 1$ (Mehta 1963). Since the dispersion velocity of particles is related to the temperature by $\sigma \sim \sqrt{T}$ and on the other hand $\sigma = \Delta \omega / \omega$, the coherent time is related to the temperature of the source as follows (Guenther 1990):

$$\tau_c \propto \frac{1}{\sqrt{T_s} \nu} \Rightarrow \tau_c = \frac{2.8 \times 10^{-4}}{\nu_{(GHz)}} \sqrt{\frac{3000}{T_s}}. \quad (13)$$

In the double slit experiment for a point-like source, in order to have diffraction pattern, the time-difference between the two light rays received by the observer should not be longer than the coherent time. Now we can constrain $f = 2kR_s$ to have diffraction features in the gravitational lensing, comparing equations (11) and (12) with the coherent time in equation (13). For the wide images we have

$$f \leq 10^6 \sqrt{\frac{3000}{T_s}}, \quad (14)$$

and for the close images we have the upper band of

$$f \leq 10^9 \sqrt{\frac{3000}{T_s}}. \quad (15)$$

For the case that $\Delta t > \tau$, the results from the wave optics reduces to the geometric optics. A more detail analysis regarding the effect of temporal coherency on the wave optics in the gravitational lensing is given in Appendix (A).

For the case of binary system composed of a parent star and a planet, we can calculating equation (7). In this system, the Fermat potential is given by

$$\phi(\mathbf{x}, \mathbf{y}) = \frac{1}{2}(\mathbf{x} - \mathbf{y})^2 - m_\star \ln(|\mathbf{x} - \mathbf{x}_\star|) - m_p \ln(|\mathbf{x} - \mathbf{x}_p|), \quad (16)$$

where m_\star and m_p are the relative mass of the star and planet normalized to the overall mass of the system and \mathbf{x}_\star , \mathbf{x}_p are the locations of lenses. We locate lenses along x_1 axis and put the center of coordinate on the center of mass of this system

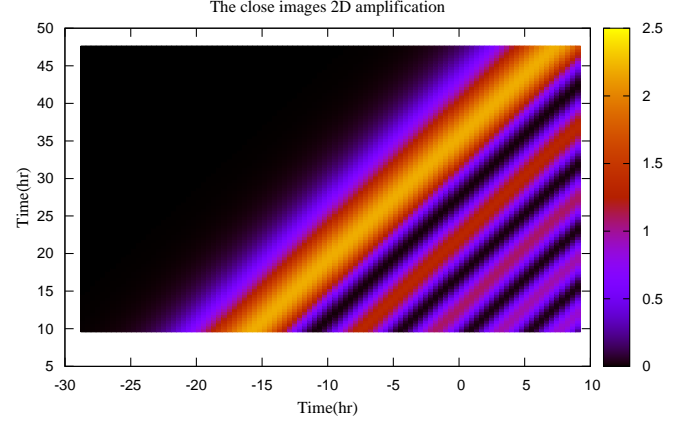


Figure 2. The two dimensional luminosity pattern from a point source on the observer plane lensed by a binary system. The fringes are demonstrated near a critical line, while the source is crossing the caustic line. The overall flux would be the sum of the nearby images (as shown in this figure) plus flux from the incoherent wide images.

$$\mathbf{x}_\star = \left(\frac{s_\perp q}{1+q}, 0 \right), \quad \mathbf{x}_p = \left(-\frac{s_\perp}{1+q}, 0 \right), \quad (17)$$

where s_\perp is the projected distance between the two lenses normalized to the Einstein radius and $q = m_p/m_\star$. The track of source on the lens plane is identified with two parameters of minimum impact parameter, u_0 with respect to the center of mass and the inclination angle of the source track α with respect to the x-axis. For the case of single lens, equation (7) has analytic solution however for two point mass, we perform numerical calculation to get the light curve. In the next section, we also do Fourier expansion of Fermat potential up some relevant terms and obtain analytical wave optics expression.

For a point source with a binary lens, using equation (7), we plot the amplification pattern as a function of time in Figure (1). This is a typical microlensing light curve with the wave optics feature. Here we have two oscillating modes due to the interference between the wide and close images. As the source gets closer to caustic line, the longer mode is magnified and after the caustic crossing it gets dimmer. In Figure (2) we depict the two dimensional pattern on the observer plane. The relative motion of the observer with respect to this pattern produces the light curve in Figure (1). In the following section, we will consider finite coherent time and finite size effects of the source star in our calculations.

2.1 Finite size effect

The majority of microlensing observations in recent years have been done towards the center of Galaxy by the two main MOA and OGLE surveys. The main aim of these two groups is discovering the extra-solar planets by the microlensing method. The source for the microlensing events in the bulge due to the selection bias are relatively populated by the red giants compare to the main sequence stars (Ansari et al. 2012). In addition to the visual band, red giants can also optically pump the interstellar medium around these stars and produce Maser emission few astronomical units far from the source star (Messineo et al. 2005;

Vlemmings et al. 2005). In contrast to the simple point like source, in reality source stars are extended objects. The extended sources not only decreases the strength of magnification in the geometric optics, it can also decrease enhancements of the fringes in the wave optics (Schneider & Schmid-Burgk 1985).

The overall intensity for the extended source in the wave optics is given by (Schneider et al. 1992) (see also equation A10 in the appendix):

$$\mu = \frac{\int_S \mu(\mathbf{y}) d\mathbf{y}}{\pi \rho^2}, \quad (18)$$

where $\mu(\mathbf{y})$ is the overall magnification of multiple images given by equation (A7) and ρ is the radius of source in terms of projected Einstein radius on the source plane.

One of the features of the finite-size effect in the wave optics is that fringes with the smaller modes in the light curve dissolve as we increase the size of the source. This effect can be seen in the Young experiment when we increase the size of pinhole as the source of double split experiment. In the gravitational microlensing, to have coherent images on the lens plane, difference between the Fermat potential of the light rays, from the different parts of the source to the images on the lens plane should not be larger than light wavelength. Assuming L_s as the size of source located at D_{ls} from the lens plane and having an image at h off-center of the optical axis, the difference between the path from the two sides of the source is

$$\Delta L = L_1 - L_2 = \sqrt{D_{ls}^2 + (h + L_s)^2} - \sqrt{D_{ls}^2 + h^2} \quad (19)$$

$$\simeq \frac{h L_s}{D_{ls}}, \quad (20)$$

since the terminal point of the light rays are fixed point on the lens plane, the gravitational potential terms have been canceled in the subtraction. Difference on in the Fermat potential is related to the difference in the light path as $\Delta L = R_s \Delta \Phi$. Imposing the condition of $\Delta L < \lambda$ and substituting from equation (20), we obtain the condition of

$$\Delta \theta < \frac{D_{ls}}{D_s} \frac{\lambda}{h}, \quad (21)$$

where $\Delta \theta$ is the apparent size of the source from the observer plane. For a single lens and high magnification events, h is in the order of the Einstein radius. We can write equation (21) in terms of the size of the source and Einstein angle as

$$L_s < \frac{D_{ls}}{D_{ol}} \frac{\lambda}{\theta_E^{(p)}} \quad (22)$$

Using the definition of the Einstein angle, upper limit on the size of the source obtain as

$$L_s < \lambda \sqrt{\frac{D_{ls} D_s}{2 R_s^{(p)} D_{ol}}}. \quad (23)$$

In order to estimate the size of source for various masses of the planets and wavelengths for the observation, we assuming lens is located at the middle of the distance between the observer and source where the probability of the microlensing observation is the highest (i.e. $D_{ol} = D_{ls}$). For two typical planets with the masses of Earth and Jupiter, the Schwarzschild radius is about 1 cm and 286 cm. Putting the source star at the Galactic bulge, $D_s = 8.5$ kpc, Table (1) shows the maximum size of the source that can produce coherent images on the lens plane. Using $\lambda = 10$ cm for the observation, we can observe the wave optics features for an earth mass planet with a typical star in the main sequence. Also we can

λ	3 cm	1 mm
$L_s(M_\oplus)$	3.4×10^6	114
$L_s(M_J)$	2.0×10^5	6.7

Table 1. Maximum size of the source in kilometer produces coherent images, located at $D_s = 8.5 \text{ kpc}$ far from the observer at the Galactic bulge observing with the two typical wavelengths of 3cm and 1mm. The calculation is done for two planets of earth mass and Jupiter mass.

observe a Jupiter mass planet having compact sources. In the micron wavelengths, our limit decreases to the ten to hundred kilometer. This means that in the smaller wavelengths for observing the diffraction pattern, we may probe smaller structures on source star such as granules (Yu et al 2011).

As we noted, in the binary lenses, distance between the two close images can be smaller than that in the single lens as the source approaches to a caustic line. For the wide images also, they form at few astronomical units far from each other. Hence at the same time we can have close coherent images from a planet companion and incoherent wide images. Hereafter, we separate magnification from the coherent and incoherent images into two parts of $A = A_{coh} + A_{incoh}$.

3 LIGHT CURVE NEAR CAUSTIC LINE

Light curve of the microlensing during the caustic crossing of the source, can be treated by numerical and analytical methods. At the position of the images on the critical lines, the lens equation is valid hence

$$\phi_1^{(0)} = \phi_2^{(0)} = 0.$$

Diagonalizing Fermat potential, we can set $\phi_{12}^{(0)} = \phi_{21}^{(0)} = 0$. In order to satisfy singular Jacobian transformation on the critical lines, from equation (6), either ϕ_{11} or ϕ_{22} should be zero. We set $\phi_{22}^{(0)} = 0$ and $\phi_{11}^{(0)} \neq 0$. Now we expand the Fermat potential around the critical line and ignore higher orders in \mathbf{x}^2 as follows (Schneider et al. 1992; Jaroszyński & Paczyński 1995):

$$\begin{aligned} \phi(\mathbf{x}, \mathbf{y}) &= \phi^{(0)} + \frac{1}{2} \mathbf{y}^2 - \mathbf{x} \cdot \mathbf{y} + \frac{1}{2} \phi_{11}^{(0)} x_1^2 + \frac{1}{6} (\phi_{222}^{(0)} x_2^3 \\ &+ \phi_{111}^{(0)} x_1^3) + \frac{1}{2} (\phi_{112}^{(0)} x_1 + \phi_{122}^{(0)} x_2) x_1 x_2 + \dots \end{aligned} \quad (24)$$

Using the Fermat principle for the critical line we demand having singular Jacobian which implies the constrain of $\phi_{122}^{(0)} x_1 + \phi_{222}^{(0)} x_2 = 0$.

The position of the source as a function of the images can be obtained from the Fermat potential as follows:

$$y_1 = \phi_{11}^{(0)} x_1 + \frac{1}{2} \phi_{111}^{(0)} x_1^2 + \phi_{112}^{(0)} x_1 x_2, \quad (25)$$

$$y_2 = \frac{1}{2} \phi_{222}^{(0)} x_2^2 + \phi_{122}^{(0)} x_1 x_2, \quad (26)$$

where keeping the first order term for y_1 and combining constrain from the Jacobin in y_2 term, we obtain the position of the images as follows:

$$\mathbf{x}_{images} = \left(\frac{y_1}{\phi_{11}^{(0)}}, \pm \sqrt{\frac{2y_2}{\phi_{222}^{(0)}}} \right). \quad (27)$$

At the negative side of the caustic we have no images and at the positive side, two images can be formed. Now we let the source just cross the caustic line with an arbitrary direction. Substituting the position of the images in equation (24), we can calculate the Fermat potential for the nearby images during the caustic crossing. The difference between the Fermat potential of two images is

$$\Delta\phi = \frac{2}{3} \frac{(2y_2)^{\frac{3}{2}}}{(\phi_{222}^{(0)})^{\frac{1}{2}}}. \quad (28)$$

Here $\Delta\phi$ is just a function of y_2 , distance to the caustic line. However in the observation of the caustic crossing the source can cross this line with an inclination, then we can replace $y_2 = \sin \gamma \times (t - t_c)/t_E$ where the time variation of $\Delta\phi$ is related to the transverse velocity and inclination angle γ as well. Using the Fermat potential for a binary system in equation (16), we can calculate $\phi_{222}^{(cm)}$ for the center of mass coordinate as follows:

$$\begin{aligned} \phi_{222}^{(cm)} = & m_p \left[\frac{6x_2}{((x_1 - x_{p1})^2 + x_2^2)^2} - \frac{8x_2^3}{((x_1 - x_{p1})^2 + x_2^2)^3} \right] \\ & + m_* \left[\frac{6x_2}{((x_1 - x_{*1})^2 + x_2^2)^2} - \frac{8x_2^3}{((x_1 - x_{*1})^2 + x_2^2)^3} \right]. \end{aligned} \quad (29)$$

Here x_1 and x_2 represent the position of critical lines where images form along these lines, depending on the location of the source, we can have double images around the parent star (wide images) or around the planet (nearby images). These double images during the caustic crossing approach to each other. Now we need performing coordinate transformation of the Fermat potential from the center of mass coordinate to the local diagonalized coordinate at the image position. First we do a boost along the x-axis to one of lens positions. The second boost is along the radial direction with size of Einstein radius corresponds to that lens. Finally we do rotation with R_{ij} to get diagonalize ϕ_{ij} . The third derivative of Fermat potential in the new coordinate system obtain as $\phi_{222}^{(0)} = R_{2i}R_{2j}R_{2k}\phi_{ijk}^{(cm)}$.

The mentioned boosts of the coordinate to the location of the images around the critical line of the planet is given by $x_1 = x_{p1} + R_E^{(p)}/R_E \cos \theta$ and $x_2 = R_E^{(p)}/R_E \sin \theta$ where $R_E^{(p)}$ is the Einstein radius of the planet and R_E is the overall Einstein radius and θ is the polar angle from the position of the planet. The order of magnitude $\phi_{222}^{(0)}$ at the position of the images would about $\phi_{ijk}^{(cm)}$ as $|R_{ij}| \sim 1$. Substituting boosts in equation (29), since $m_* \gg m_p$, first term can dominate as $R_E^{(p)}$ appears in the denominator, hence

$$\phi_{222}^{(0)} \simeq -m_p \left(\frac{R_E^{(p)}}{R_E} \right)^{-3}.$$

Replacing the ratio of Einstein radius of the planet to the Einstein radius of the star with corresponding masses and using normalized planet mass with $m_p = q/(1+q)$, results in

$$\phi_{222}^{(0)} \simeq -\frac{1}{\sqrt{q}}. \quad (30)$$

Intuitively, comparing the double images around the planet and the lensing star, nearby images around the planet is more suitable for producing the diffraction pattern. Having smaller q makes larger $\phi_{222}^{(0)}$

Now we substitute equation (30) in equation (28) and replace the difference in the Fermat potential to the time difference as follows:

$$\Delta t = 2 \times R_s \Delta\phi$$

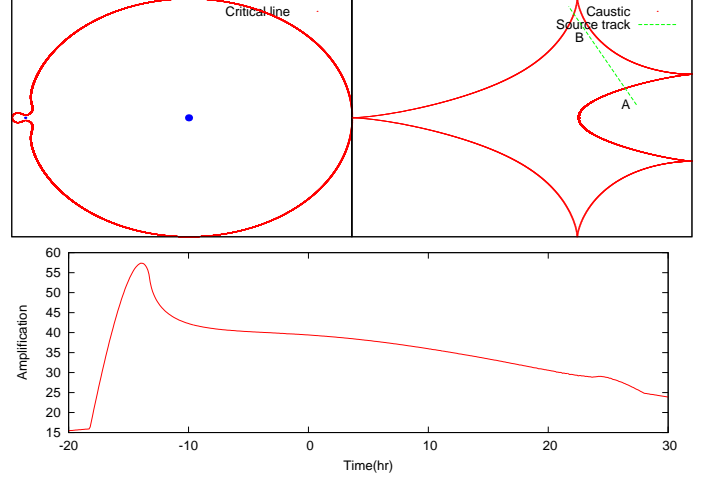


Figure 3. Critical lines (left panel), caustic lines (right panel) and light curve in the geometric optics (lower panel) for a binary system with the parameters of $q = 0.001$, $s_{\perp} = 1$. Here we take source star with the size of $\rho = 0.002$. Large loop around the primary lens corresponds to the parent star and smaller loop corresponds to the planet. The straight solid line indicates the path of the source.

$$\begin{aligned} &= 5 \times 10^{-9} \\ &\times \left(\frac{t - t_c}{1h} \sin \gamma \right)^{3/2} \left(\frac{t_E}{40days} \right)^{-3/2} \left(\frac{q}{0.001} \right)^{1/4} \left(\frac{M}{M_{\odot}} \right) sec \end{aligned}$$

where $(t - t_c)/1h$ is the time corresponds to the relative velocity of the source on the lens plane normalized to one hour. We note that unlike to the case of single lens where Δt is in the order of crossing time of the Schwarzschild radius, in the case of binary lens we have the factor of q , decreases the corresponding time (Heyl 2010). On the other hand Δt approaches to zero as $t \rightarrow t_c$. The characteristic time difference in the Fermat potential is about $\Delta t \sim 5 \times 10^{-9}$ sec corresponds to $l_{th} \sim 15$ cm. This length scale corresponds to the frequency of 0.2 GHz. Here wavelengths larger than this threshold l_{th} , can interfere and produce the diffraction pattern from the images on the source plane.

Repeating this calculation for the distant images around the parent star, we get a larger value for Δt , destructive for the wave optics feature. The other observable parameter which depends on the position of the images is the amount of the magnification during the lensing. Substituting equation (24) in equation (7), and keeping leading terms in the Fermat potential, the magnification near the caustic obtain as follows (Schneider et al. 1992):

$$\mu \sim [Ai(\frac{y_2}{Y_0})]^2, \quad (31)$$

where $Y_0 = (\frac{|\phi_{222}^{(0)}|}{2f^2})^{\frac{1}{3}} \sim q^{-1/6}$ and $Ai(x)$ is Airy function. The maximum magnification also relates to the derivatives of Fermat potential as $\mu_{max} \propto |\phi_{11}^{(0)}|^{-1} |\phi_{222}^{(0)}|^{-2/3} \sim q^{1/3}$. Near the critical line for the nearby images, having larger $\phi_{222}^{(0)}$ makes smaller amplitude for the diffraction light curve and larger Y_0 produces longer modes. On the other hand for the distant images around the lens star, q is large, results in smaller $\phi_{222}^{(0)}$ and smaller diffraction pattern with larger magnification (i.e. closer to the geometric optics). We remind that in our diagonalized coordinate system for the Fermat potential, the non-zero term of the second order derivative of the Fermat potential is ϕ_{11} . On the other hand the trace of ϕ_{ij} is $\nabla^2 \phi = 2 - \nabla^2 \psi$, where for two point mass lenses the second term

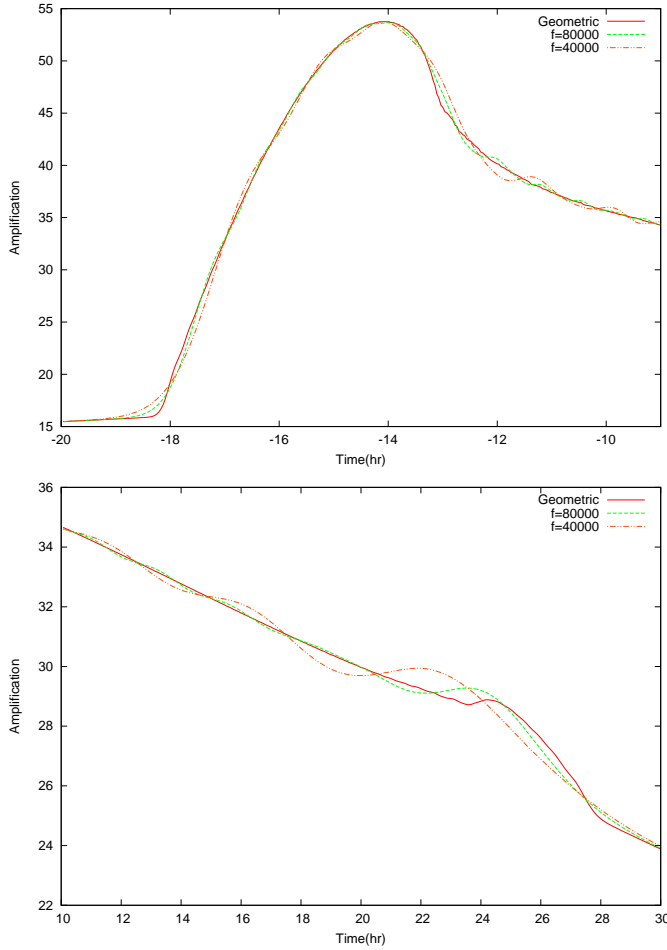


Figure 4. The light curves correspond to the wide images (upper panel) and close images (lower panel) around the lens star and planet, crossing the caustic lines at point *A* and *B* of Figure 3. The solid line corresponds to the geometric optics, with the two wave optics light curves at 5 and 60 MHz frequencies.

is a delta-Dirac function and can be set to zero along the caustic lines, far from the position of the lenses. Hence for a small distance from the caustic lines, $\phi_{11} = 2$. Therefore, the relevant parameters in the light curve of the wave optics are f , ϕ_{222} and the trajectory of the source with respect to the caustic line.

Figure (3) shows the configuration of a binary lens (parent star with the planet) with the corresponding critical lines and caustic lines and the light curve in the geometric optics. Caustic crossing happens at two points of *A* and *B* produces nearby and distant images. Figure (4) shows corresponding light curve in the wave optics and geometric optics in two wavelengths at the points *A* and *B*. The light curves have been obtained from the numerical Fresnel-Kirchhoff integration. The analytical approach in this section revealed us the physics of the wave optics in the gravitational microlensing by a binary system. For full analysis of the light curves we will use the numerical calculation in the next section.

4 OBSERVATIONAL PROSPECT

In this section we study the possibility of follow-up observations of a binary microlensing system during the caustic crossing by a radio telescope, such as future SKA project. In a simple lens, the parameters involve in the light curve are the Einstein crossing time t_E , minimum impact parameter u_0 and time for the maximum magnification t_0 . Amongst these parameters, the only parameter that has the physical information of the system is t_E which contains the mass of lens, relative distance of the lens with respect to the source and the transverse speed of the lens with respect to our line of sight. Using additional information as parallax effect due to the annual motion of the earth around the sun (Gould 1998) can break the degeneracy between the lens parameters (Rahvar et al. 2003). On the other hand the finite size effect of the source can also provide extra information to break partially the degeneracy of the problem (Roulet & Mollerach 1997).

Increasing the number of lens from one to two, increases the number of parameters of this system. The additional parameters are (i) the projected distance between the lenses normalized to the Einstein radius, " s_\perp ", (ii) relative mass of the lenses, " q " and (iii) angle " α " defining the trajectory of the source with respect to the line, joining two lenses. For the binary system, we have overall six parameters to fit the light curve. The probability of observation of the binary lenses depends on the size of the caustic and for the case of resonance where the distance between the lenses is in the order of Einstein ring, we will have the maximum probability. However the problem with the resonance events is that despite of occasional observation of planets, due to lack of our complete knowledge about the observational efficiency, it is difficult to have a statistical analysis and extract the distribution function of the planet parameters. There are some efforts to have a fully-deterministic strategy by automated searching system to have the detection efficiency of the exoplanets (Dominik et al 2010). Having such a system to cover all the alerted microlensing candidates will enable us to get correct statistical distribution of the planet parameters.

The other important channel for the exoplanet observation is the high magnification events (Griest & Safizadeh 1998). These events due to the high magnification character are alerted by the microlensing surveys and the follow-up telescopes could monitor them with high sampling rate and better photometric precision. Unlike to the low magnification events, for these events, the detection efficiency function is almost known and the statistical analysis of the planet distribution can be applied (Gould et al. 2010). However these events suffer from $s \leftrightarrow s^{-1}$ degeneracy, where we can have the same light curve for the close and wide caustic configurations. In the caustic classification of the binary systems there are three type of topologies for the caustics and corresponding critical lines (Schneider & Weiß 1986), so-called the "close", "wide" and "intermediate" or resonance binaries. Figure (5) shows these three categories of caustic lines with three different planet to the star mass ratio. For studying the wave optics feature during the caustic crossing, we generate synthetic light curves for the three different categories and compare the results with the geometric optics. Our aim is also to study the sensitivity to wave optics signals in the resonance and high magnification channels.

In order to quantify the wave optics feature in the light curve, we use χ^2 difference from the best fit of wave optics and geometric optics. Assuming σ_i as the error bar for each data point, $\mu_i^{(g)}$ as the magnification in the geometric optics and $\mu_i^{(w)}$ as the magnification

in the wave optics, the difference between the χ^2 s is given by

$$\begin{aligned} \Delta\chi^2 &= \chi_{g.o.}^2 - \chi_{w.o.}^2 \\ &= \sum_{i=1}^N \frac{1}{\sigma_i^2} (\mu_i^{(w)} - \mu_i^{(g)}) (2\mu_i^{(exp)} - \mu_i^{(w)} - \mu_i^{(g)}). \end{aligned} \quad (32)$$

Having a threshold for $\Delta\chi^2$, we can distinguish the wave optics light curve from the geometric optics. An important factor for determining equation (32) is knowing the photometric error bar which depends on the source flux, integration time and the size of the radio telescope. Amongst the various sources, red giants and supergiants can emit electromagnetic waves in the longer wavelengths. Radio-loud Quasars at the cosmological scales are also bright radio sources where caustic crossing features can be observed in the cosmological scales.

Detail study about the radio sources have been done for the wave optics microlensing in Heyl (2011). In what follows we adapt his classification. For the red giants a closer star as Arcurus (Perryman et al. 1997) shows emission at the wavelengths of 2cm and 6cm has 0.68 mJy and 0.28 mJy flux, respectively (Drake & Linsky 1986) and its spectrum is given by

$$f_\nu \simeq 24 \left(\frac{\nu}{GHz} \right)^{0.8} \left(\frac{kpc}{D_s} \right)^2 nJy. \quad (33)$$

Another class of stars are low mass late-type stars as asymptotic giants. For example, Mira is a sample of this class and the spectrum is given by (Perryman et al. 1997; Reid et al. 1997)

$$f_\nu \simeq 72 \left(\frac{\nu}{GHz} \right)^2 \left(\frac{kpc}{D_s} \right)^2 nJy. \quad (34)$$

Finally super giants have strong radio emission. Betelgeuse is one of the red super giants that is located at the distance of 197 pc (Newell & Hjellming 1982; Harper et al. 2008). The spectrum of this star normalized to the kilo-parsec distance is given by

$$f_\nu \simeq 9.3 \left(\frac{\nu}{GHz} \right)^{1.32} \left(\frac{kpc}{D_s} \right)^2 \mu Jy. \quad (35)$$

The radius of super giants are in the order of a few astronomical unit. Assuming these stars located at the Galactic center, about eight kpc far from us, from equation (21), we can have coherent images for the close images on the lens plane.

In equation (32), we need an estimation for the photometric error bar. For the SKA project the noise corresponds to Nyquist sampling is 0.27 Jy (Schilizzi et al. 2007). This sampling is defined according to the integration time multiplied to the band width to be equal to one (i.e. $\Delta\nu \Delta\tau = 1$). Since noise decreases with the square root of time and band width as $1/\sqrt{\Delta\nu \Delta\tau}$, we can write the noise in terms of these two parameters as follows

$$\Delta f = 0.14 \left(\frac{\Delta\nu}{GHz} \right)^{-1/2} \left(\frac{\Delta\tau}{1hr} \right)^{-1/2} \mu Jy. \quad (36)$$

Now we use six parameters of the microlensing in the binary system as well as the source stars listed before for generating synthetic light curves with the corresponding error bars. In order to compare the simulated data with the geometric and wave optics light curves, we use the criterion of $\Delta\chi^2 > 5$. For an ensemble of light curves, we identify the caustic lines in the three categories of binaries as shown in Figure (5). Those light curves cross the caustic lines and satisfy the discrimination criterion between the geometry optics and wave optics are identifies in this figure. Results show that wave optics feature is just depends on the location of the source crossing the caustic lines.

As we noted before, there are two main channels for the ex-

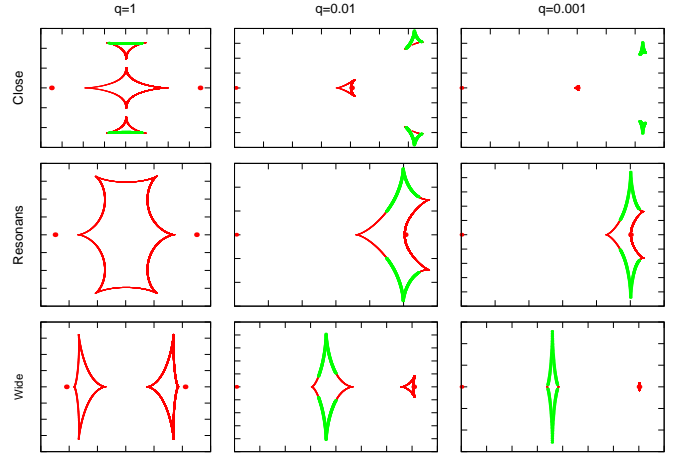


Figure 5. Caustic lines for three category of wide, close and intermediate separation of the lens from the planet with different values of q . The thick green area of the caustic lines produces light curves with $\Delta\chi^2 > 5$ from equation (32). The binary lenses are indicated by two spots and scales in the figures are given in terms of distance between the lenses.

oplanet observations and a qualitative study of wave optics light curves can be done by studying Figure (5). For the case of high magnification events, the source passes near the lens star. Having small q , wide and close binaries can produce almost same light curves and according to Figure (5), we will not have strong wave optics features for this case. On the other hand for the intermediate regime (resonance) a larger area of the caustic lines is suitable for the wave optics light curve. For this case, we will have combination of both close and wide images on the lens plane.

Amongst the light curves we generated in the Monte-Carlo simulation, a sample of light curve is shown in Figure (6) with the cadence rate of 45 min and signal to the noise ratio of $S/N = 7$. Here the solid line indicates the geometric optics and the dotted line is theoretical wave optics light curves. The relevant parameters of the wave optics from equation (31) are the wavelength in the Airy function, Y_0 and maximum amplitude of the light, μ_{max} . However these parameters also depend on f and ϕ_{222} . For an ensemble of the light curves with uniformly distribution in the parameter space, we calculate $\Delta\chi^2$ between the wave optics and the geometric optics as in equation (32). In order study relation between the discriminating parameter, $\Delta\chi^2$ with f and ϕ_{222} , we specify areas in this parameter space, satisfying $\Delta\chi^2 > 10$ with the source sizes of $\rho = 0.001, 0.005$ and 0.002 , in Figure (7). Upper part of these curves are excluded. Having smaller f means longer wavelength for the observation of small mass lens. On the other hand larger ϕ_{222} is also relates to the wave optics from the time difference between the images. Smaller size sources satisfying the spatial coherency are suitable for the wave optics microlensing. Knowing the transit time scale of the fringes changes with respect to the observer $\Delta\tau$, we can determine $Y_0(f, \phi_{222}^{(0)}) = \Delta\tau/t_E$. On the other hand $\mu_{max}(\phi_{222})$ can be measured directly from the light curve.

The physical parameters involve in the wave optics light curves are the overall mass of the system M_t , q and the angle of the source trajectory, α . On the other hand from the observations in the visual telescopes, we can find the best light curve fit with six parameters of the theoretical model and possible degrees of degeneracy. Having extra information from the wave optics will constrain

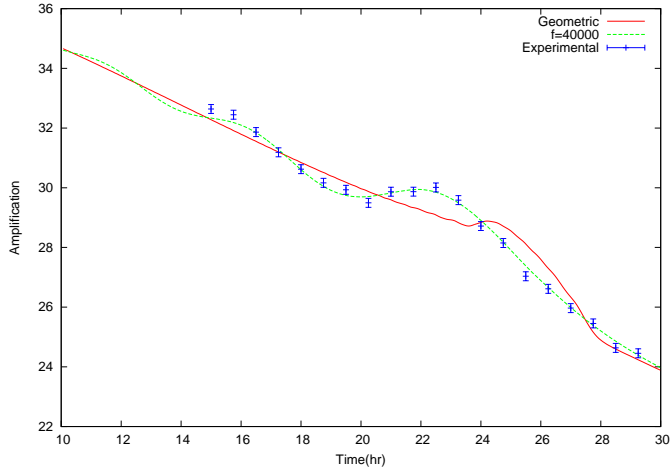


Figure 6. A part of theoretical light curve from the geometric and wave optics. The data points are simulated according to the amount of noise from SKA. Here we take $\frac{S}{N} = 7$. The parameters of the lens is similar to that in Figure (4) with the observational frequency of 10 GHz frequency and 45 minute integration time.

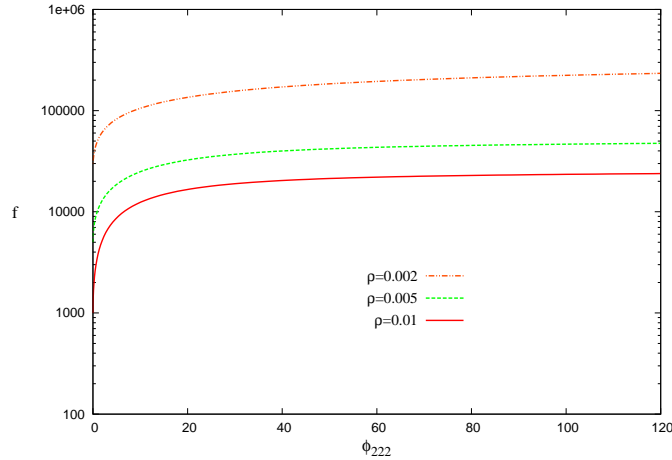


Figure 7. Area above the curves in parameter space of $(f - \phi_{222})$ space has been excluded for having wave optics features with the criterion of $\Delta\chi^2 > 10$. The size of the source star normalized to the Einstein radius is mentioned in the legend of Figure. Smaller stars are favorable for the wave optics microlensing.

M_t , q space and subsequently we can have better confidence from measurement of s_{\perp} .

Now we want to examine the sensitivity of the wave optics signals to the main physical parameters of the binary system, q and s_{\perp} . In our Monte-Carlo simulation, we can identify percentage of the events that satisfy the condition of $\Delta\chi^2 > 10$. According to Figure (8), the fraction of events is given in terms of percentage and suitable area of the parameter space for the wave optics signals is in the resonance region where the separation between the lens and planet is around the Einstein radius. The physical reason as we discussed in Figure (5), is that in the intermediate regime, the close images favorable for the wave optics features can be formed. In order to estimate the overall number of the microlensing events

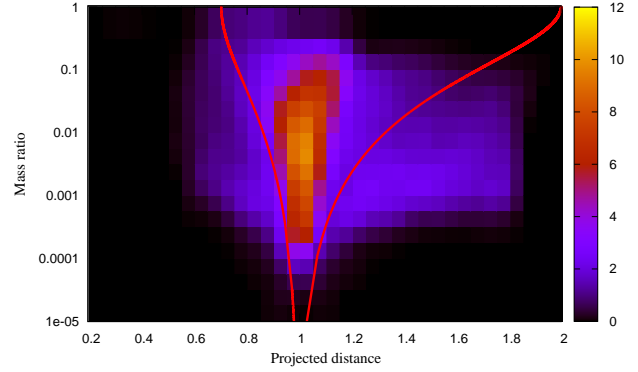


Figure 8. Efficiency function in s, q space that can produce wave optics features on the observer plane. The criterion for the wave optics from equation (32) is taken $\Delta\chi^2 > 10$. The simulation is done for the source star with the finite size of $\rho = 0.005$ and observation at the frequency of $\nu = 10 \text{ GHz}$. The six parameters of the lens are generated with the uniform distribution. Red lines separate the parameter space according to the definition of the wide, close and intermediate binaries from Erdl & Schneider (1993).

with the wave optics signal, we should multiply this histogram to the diagram contains the abundance of the binary events.

Finally we want to extract the physical information from a typical wave optics light curve, assuming that observation is done both in the visual and radio wavelengths. From the visual wave length observation, fitting with the geometric optics we can extract q and s_{\perp} and trajectory of the source. On the other hand from the wave optics our relevant variable are f and $\phi_{222} \sim 1/\sqrt{q}$.

In what follows we assume a synthetic data taken by the radio observation along with the geometric observation in the visual band. Here parameters of the lens as the apparent distance between the lenses as well as the mass ratio and trajectory of the source can be obtained from the geometric optics, however there is a degree of degeneracy in the best fit to the data. From the wave optics the degree of freedom appear in the light curve is f which relates to the total mass of the lenses. This parameter can be fixed by the wave optics observation and subsequently the total mass of the system can be identified. In Figure (9) we fit the synthetic data with the theoretical wave optics light curve. Here the theoretical value of f is 49475 and assuming observation at $\nu = 10 \text{ GHz}$, from the likelihood function we get $f = 51400^{+1635}_{-1600}$. Using k in the definition of f , we can extract the overall mass of the binary system.

5 CONCLUSION

In this work we study the wave optics effect of the gravitational microlensing by a binary system composed of lens star and companion planet. Having planet in the lensing system causes generating close images during the caustic crossing, a suitable configuration of the images on the lens plane to produce diffraction pattern. This effect is in analogy to the double slit Young experiment in the astronomical scales. We derived the light curve for the binary system in the framework of the wave optics showing that it depends on the derivatives of the Fermat potential and f .

Taking red giants and supergiants as the source stars of the

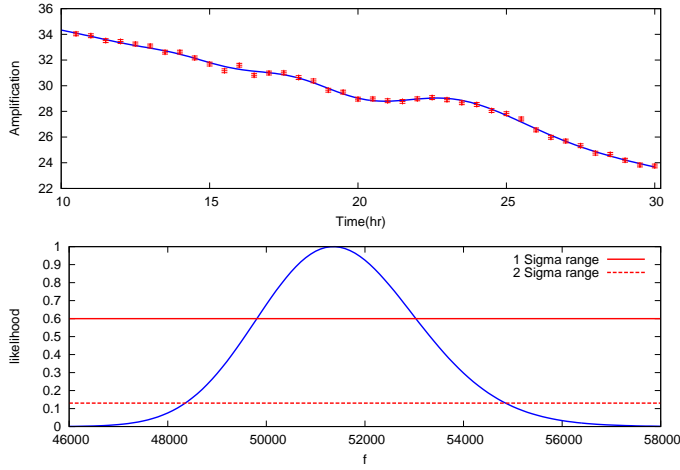


Figure 9. Synthetic light is generated by the cadence of 30 min and photometric precision of 0.15, fitted with the wave optics theoretical light curve. The initial value of f is taken 49475, using $\nu = 10\text{GHz}$ observational frequency. The likelihood function shows the best fit with 1σ and 2σ level of confidences. With 1σ , we obtain $f = 51400^{+1635}_{-1600}$

gravitational microlensing in the galactic scales where there is a natural preference for observing these type of sources in the microlensing, we suggestion using SKA future project for the observation of wave optics signals in the light curve. In this observational program, radio observations can accompanying the microlensing follow-up telescopes in the visual bands towards the center of Galaxy. These two observations in the long and the shorter wave lengths can be a complimentary observations of the binary microlensing events, result is breaking the possible degeneracy of binary system. Amongst two observational channels for the exoplanet observation by the microlensing so called (i) high magnification channel and (ii) resonance channel, we showed that wave optics observations is applicable for the resonance events where a larger area of the caustic lines is favorable for manifestation of the wave optics microlensing. Finally we discuss on sample of synthetic microlensing light curves and application of wave optics and geometric optics to identify the parameters of the lens with the better accuracy.

ACKNOWLEDGMENTS

AM thanks Sharif university of Technology providing high performance computational facilities. We also thank Avery Broderick for his useful comments.

REFERENCES

- Ansari, R., Moniez, M., Perdereau, O., Rahvar, S., in preparing for submission to A&A.
 Arnold, V. I., *Mathematical Methods of Classical Mechanics*, 2nd edition, Springer-Verlag, New York.
 Born, M., Wolf, E., *Principles of Optics*, Cambridge University Press. 7th edition, 2002.
 Dominik, M., 2007, MNRAS, 377, 1679
 Dominik, M., Jørgensen, U. G., Rattenbury, N. J., et al. 2010, *Astronomische Nachrichten*, 331, 671

- Drake S. A., Linsky J. L., 1986, *Astron. J*, 91, 602
 Erdl, H., & Schneider, P. 1993, *A&A*, 268, 453
 Einstein A., 1936, *Science*, 84, 506
 Gould, A., 1998, *ApJ*, 506, 253
 Gould, A., Dong, S., Gaudi, B. S., et al. 2010, *ApJ*, 720, 1073
 Griest, K., & Safizadeh, N., 1998, *ApJ*, 500, 37
 Guenther, B. D., *Modern Optics*, Wiley, 1990
 Harper, G. M., Brown A., Guinan, E. F., 2008, *Astron. J*, 135, 1430
 Heyl, J. S., 2010, MNRAS, 402, L39
 Heyl, J. S., 2011, MNRAS, 411, 1780
 Heyl, J. S., 2011, MNRAS, 411, 1787
 Jaroszyński, M., Paczyński B., 1995, *ApJ*, 455, 443
 Mandzhos, A. A., 1981, *Pis'ma. Astron. Zh.*, 7, 387
 Mao, S., & Paczynski, B., 1991, *ApJ*, 374, L37-L40
 Mao, S., Paczyński, B., 1991, *ApJ*, 374, L37.
 Mehta, C., 1963, *Nuovo Cimento*, 28, 401
 Messineo, M., et al., 2005, *A&A*, 435, 575
 Newell, R. T., Hjellming, R. M., 1982, *Astrophys. J Lett*, 263, L85
 Ohanian, H. C., 1983, *ApJ*, 271, 551
 Paczyński, B., 1986, *ApJ*, 304, 1
 Perryman, M. A. C., et al., 1997, *Astron. Astrophys.*, 323, L49
 Rahvar, S., Moniez, M., Ansari, R., & Perdereau, O., 2003, *A&A*, 412, 81
 Reid, M. J., Menten, K. M., 1997, *Astrophys. J*, 476, 327
 Roulet, E., & Mollerach, S., 1997, *Physics Report*, 279, 67
 Schilizzi, R. T., et al., 2007, Technical report, Preliminary Specifications for the Square Kilometre Array.
 Schneider, P., Weiß, A., 1986, *A&A*, 164, 237
 Schnieder, P., & Schmid-Burgk, J., 1985, *A&A*, 148, 369
 Schneider, P., Ehlers, J., Falco, E. E., *Gravitational Lenses*, Springer-Verlag, Berlin, Heidelberg, New York, 1992
 Vlemmings, W. H. T., et al., 2005, *Memorie della Societ Astronomica Italiana*, 76, 462
 Walsh, D., Carswell, R. F., Weymann, R. J., 1979, *Nature*, 279, 381
 Yu, D., Xie, Z., Hu, Q., et al. 2011, *ApJ*, 743, 58
 Zabel, S. A., Peterson, J. B., 2003, *The Astrophysical Journal*, 594, 456

APPENDIX A: COHERENCY IN THE WAVE OPTICS: GRAVITATIONAL LENSING

In order to show the effect of coherent time on the wave optics in the astronomical scale, we compare the time delay between the light rays arriving to the observer with the source coherent time. We adapt the wave optics formalism in Schneider et al. (1992). Starting from the amplitude of the electromagnetic field on the lens plane, it can be obtained on the observer plane as

$$V = \int e^{if\phi(x,y)} dx^2. \quad (\text{A1})$$

Doing the Taylor expansion of the Fermat potential around the image at the stationary point and diagonalizing the Fermat potential results in

$$V = \int e^{if[\phi^{(0)} + \frac{1}{2}(\phi_{11}^{(0)} x_1^2 + \phi_{22}^{(0)} x_2^2)]} dx^2. \quad (\text{A2})$$

The integration of equation (A2) is

$$V = \frac{2\pi i}{f} \frac{1}{\sqrt{\det |J|}} e^{if(\phi^{(0)} - n_i \phi/2)} \quad (\text{A3})$$

where $\det |J|$ is the determinant of ϕ_{ij} in equation (6), in the diagonalized coordinate and n refers to the type of images and can be $n = 0, 1, 2$, depending on the number of focal points transverse from the source to the observer (Arnold 1989). Now if we have N images from the lensing, the overall amplitude would be

$$V = \frac{2\pi i}{f} \sum_{i=1}^N \frac{e^{i(f\phi_i^{(0)} - n_i\pi/2)}}{\sqrt{|\det J_i|}}. \quad (\text{A4})$$

We note that this equation is valid while the source is out of the caustic lines (i.e. $\det |J_i| \neq 0$). If we take into account the spectrum for the source, replacing f with $2\omega R_s$, the overall amplitude is given by

$$V = \frac{2\pi i}{f} \sum_{i=1}^N \frac{1}{\sqrt{|\det J_i|}} \int e^{i(2R_s\omega\phi_i^{(0)} - n_i\pi/2)} g(\omega) d\omega. \quad (\text{A5})$$

The overall magnification is given by equation (7), hence the overall magnification after averaging over the time is given by

$$\begin{aligned} \mu &= \sum_{i=1}^N \mu_i \\ &+ \sum_{i \neq j} \sqrt{\mu_i \mu_j} \int g(\omega)^2 e^{i[2R_s\omega(\phi_i^{(0)} - \phi_j^{(0)}) - \frac{\pi}{2}(n_i - n_j)]} d\omega. \end{aligned} \quad (\text{A6})$$

The argument in the phase is $f(\phi_1^{(0)} - \phi_2^{(0)}) = \omega \Delta t$, assuming a Gaussian spectrum for the source, for the case that the temporal coherent time is shorter than the time difference between the light rays, the cross terms will be zero and we reach to the geometric optics. For the simple case of two images, $N = 2$, putting a Gaussian spectrum for $g(\omega)$, we obtain the following result for the magnification

$$\mu = \mu_1 + \mu_2 + 2e^{-(\frac{\Delta t}{\tau})^2} \sqrt{\mu_1 \mu_2} \cos[\omega_0 \Delta t - \frac{\pi}{2}(n_1 - n_2)], \quad (\text{A7})$$

here we replace the width of the spectrum with the coherent time as follows $\Delta\omega = \frac{1}{\tau}$. For $\Delta t \ll \tau$, we have an oscillating mode, reveals the wave optics feature from the superposition of the waves. In contrast, for $\Delta t \gg \tau$ the exponential term vanishes the oscillating term and we will have geometric pattern for the magnification.

In the case of extended source, each point on the source has contribution on every point of the observer plane. Hence we for this case we can write equation (A5) for each point of source assigning it by $V(s)$. The overall amplitude can be written as

$$\begin{aligned} |V|^2 &= \left(\frac{2\pi}{f}\right)^2 \frac{1}{S^2} \int \int \sum_{i,j=1}^N \frac{ds ds'}{\sqrt{|\det J_i(s)| |\det J_j(s')|}} \times \\ &\int \int e^{i[R_s(\omega\phi_i^{(0)}(s) - \omega'\phi_j^{(0)}(s')) - (n_i - n_j)\pi/2]} <g(\omega)g(\omega')> d\omega d\omega'. \end{aligned} \quad (\text{A8})$$

where S is the area of the source and averaging is taken over the time, hence $<g(\omega)g(\omega')> = g(\omega)^2 \delta(\omega - \omega')$. Since the differential elements on the source are spatially uncorrelated, the cross terms in equation (A8) from the different elements will be canceled and only light rays propagating from one element of the source contribute in this summation. Mathematically we may consider

$$<\phi_i^{(0)}(s)\phi_j^{(0)}(s')> \sim \delta(s - s').$$

Hence equation (A8) can be simplified to

$$\mu = \frac{1}{S} \int ds \int \sum_{i,j=1}^N \frac{e^{i[R_s\omega(\phi_i^{(0)}(s) - \phi_j^{(0)}(s)) - (n_i - n_j)\pi/2]}}{\sqrt{|\det J_i(s)| |\det J_j(s)|}} g(\omega)^2 d\omega, \quad (\text{A9})$$

and simplifying this equation results in

$$\mu = \frac{1}{S} \int \mu(s) ds \quad (\text{A10})$$